Spark Plasma Sintering of Nano Silicon Carbide Reinforced Alumina Ceramic Composites

Mustafa Guven Gok

Hakkari University, Engineering Faculty, Materials Science and Eng. Department, Turkey

Abstract

Although Al_2O_3 has been commercially preferred material, it cannot be used in applications subject to variable and sudden loads due to its low fracture toughness. In this study, as the primary purpose, nano-SiC particles were used as reinforcement phase to improve the fracture toughness of the Al_2O_3 ceramic. Ultrasonic dispersion was used to ensure good dispersion of the nano reinforcement phase in the matrix. Production was carried out by spark plasma sintering method at temperatures of 1325 °C for 5 min under 40 MPa pressure and vacuum atmosphere. Densification behavior, density, microstructure, phase analysis, hardness and fracture toughness of the sintered Al_2O_3/nano-SiC composites were investigated. The highest hardness and fracture toughness of 22.83 GPa and 6.09 MPa·m$^{1/2}$ were achieved, respectively.

Keywords: Spark Plasma Sintering; Al_2O_3; Nano-SiC; Ceramic Composite; Fracture Toughness.

1. INTRODUCTION

Alumina (Al_2O_3), as an engineering ceramic, has high melting temperature (2072 °C), high hardness, low density (3.9 gr/cm^3) and low thermal conductivity. In addition, its corrosion resistance and biocompatibility are very good. Thanks to these features, it has a high potential to be used in a number of sectors such as aerospace and automotive industries, ballistic armor applications, high temperature refractory materials, cutting and abrasive tools and biomaterials. However, fracture toughness value of Al_2O_3, which is resistance to crack propagation, is quite low [1-5]. This negative feature limits the use of Al_2O_3. On the other hand, there are many studies to increase the fracture toughness of Al_2O_3 based ceramics through microstructure control and reinforcement phase mechanisms [1, 3, 4, 6–9]. The reinforcement phase mechanism of Al_2O_3 matrix is occurred by secondary phases in the forms of particle and/or fiber. Thus, a composite material is produced. As shown schematically in Figure 1, the main purpose of the reinforcement phase mechanism is to reduce the energy of the crack propagating in the matrix. In the crack deflection mechanism given in Figure 1 (a), as the crack moves through the material, when it intersects with the reinforcement particles, the direction of the crack propagation plane changes and its energy decreases. In the other mechanism called as crack branching (Figure 1 (b)), the crack intersecting with the reinforcement particles splits into two or more cracks and its energy decreases. In the case

of crack bridging mechanism shown in Figure 1 (c), the reinforcement phase in the form of fiber acts like a spring trying to close the crack and prevents further spreading the crack.
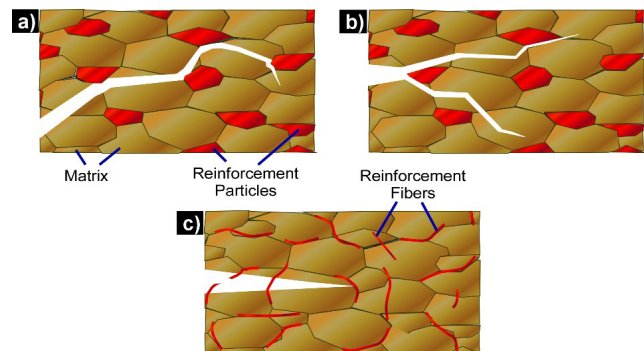
Figure 1. Schematic explanation of the improvement in the fracture toughness through reinforcement phases; crack deflection (a), crack branching (b), crack bridging (c).

When silicon carbide (SiC) is selected as the ceramic reinforcement phase, significant improvements in mechanical properties of the Al_2O_3 are possible [10]. At this point, it is reported that the amount, size, morphology and distribution of SiC phase added into the alumina matrix has a great effect on the mechanical properties of Al_2O_3 [11]. Razavi et al. [10] produced the Al_2O_3-SiC composite ceramics by using spark plasma sintering (SPS) method at temperatures of 1600 °C for 10 min holding time and they measured the hardness and fracture toughness values of the monolithic Al_2O_3 as 1387 Hv and 250.4 MPa, respectively. Researchers showed that hardness of the composite containing 20 wt. %

SiC increased to 2329 Hv and flexural strength of the composite containing 10 wt. % SiC increased to 293.1 MPa. In another study [11], A_2O_3-SiC composite containing 17 vol. % SiC was produced by SPS method (1550 °C temperature, 80 MPa pressure and 30 min. holding time) and its hardness value measured as maximum 21.7 GPa. Saheb et al. [2] produced the Al_2O_3-SiC-CNT composites using the SPS method at 50 MPa pressure, 1500 °C sintering temperature and 10 min. holding time. As a result, they showed that while the fracture toughness value of monolithic Al_2O_3 was 3.61 MPa.$m^{1/2}$, this value increased to 6.98 MPa.$m^{1/2}$ in the composite of Al_2O_3-10SiC-2CNT (vol. %). In the study conducted by Alweendo et al. [12] determined the hardness and fracture toughness values of the monolithic Al_2O_3 produced by SPS method as 15.8 GPa and 4.2 MPa.$m^{1/2}$, respectively. They also showed that it was possible to increase the hardness and fracture toughness up to 16.1 GPa and 4.7 MPa.$m^{1/2}$, respectively, by adding 10 % SiC by volume.

On the other hand, although there are other pressure and non-pressure sintering processes in ceramic composite production, SPS is one of the newest and technological methods in the production of engineering ceramics. In this method, heat is produced directly on the powders and the molds thanks to the electric current applied in the form of square wave pulses that can be controlled completely, and therefore, the sintering temperature can be reached in a very short time. During the process, pressure is applied to the powders and the microstructure can be controlled by high heating rate [10, 11].

In this study, Al_2O_3/nano-SiC composites containing different ratio of nano-SiC particles (0-30 vol. %) were produced by using spark plasma sintering process. To achieve good dispersion, the nano-SiC particles were dispersed ultrasonically in the Al_2O_3 matrix. The effects of nano-SiC ratio on densification behavior, microstructure, mechanical properties and phase structure of composites were investigated.

2. MATERIAL AND METHODS

2.1. Powder Preparation

Firstly, commercial Al_2O_3 (*US Research Nano Materials, USA, an avarage particle size 500 nm, alpha, 99+%*) and (*US Research Nano Materials, USA, 45-65 nm, beta, cubic, 99+%*) SiC powders were weighed in the proportions given in Table 1. Then, the nano SiC powders were added to the merck quality ethanol in separate beakers. An ultrasonic probe (Heiscer-UP200Ht) was placed in beakers containing ethanol and nano SiC powders, and dispersion of nano-sized powders in ethanol was provided for 15 minutes. The process was continuously controlled so that the ethanol in the beaker did not overheat, the ethanol was kept cold with the aqueous system placed under the beaker, and the temperature of the system was measured with a thermometer. After the distribution of nano-sized powders, Al_2O_3 powders were added to the same beakers in appropriate proportions and ultrasonic dispersion was performed for another 15

minutes. Then, magnetic stirring bars were placed to the beakers and the ethanol evaporated on a magnetic stirrer having heater and vacuum fan. The beakers were placed in a drying-oven at 80 °C to dry the powders completely.

Table 1. Sample Compositions.

Specimen Name	Amount of Powder (vol. %)	
	Al_2O_3	SiC
100A	100	-
90A10S	90	10
80A20S	80	20
70A30S	70	30

2.2. Spark Plasma Sintering Process

Prepared powders were sintered by using spark plasma sintering process. A SPS system (7.40 MK VII, SPS Syntex Inc.) with a capacity of 20000A was used. Thanks to this system, composite specimens with 50 mm diameter and 5 mm thickness were produced as shown in Figure 2. Graphite molds having 50 mm inner-diameter and graphite punches were used for composite production. The inner surface of the mold was covered with graphite paper, the lower punch was placed and graphite papers were placed both on the surfaces of upper and lower punches. The powder to be sintered was poured into mold cavity and upper punch placed. Then, the graphite mold was pre-compressed under 10 MPa pressure by using a hand press. In order to minimize heat loss, the graphite molding system was surrounded by a graphite blanket and sintering carried out in a vacuum environment. During SPS process, current was increased manually and shrinkage curves were controlled continuously. 40 MPa pressure was applied to the punches and pulsed direct current (12 ms/on, 2 ms/off) was passed through the samples and graphite molds during sintering process. The process was completed by holding the specimens 5 minutes at temperature of 1325 °C. Temperature measurements were performed by a pyrometer from the outside of chamber. During sintering, a software was used to control instant parameters such as shrinkage, shrinkage rate, temperature, vacuum value, current, voltage and pressure, and a heating rate of 150 °C/min was applied.
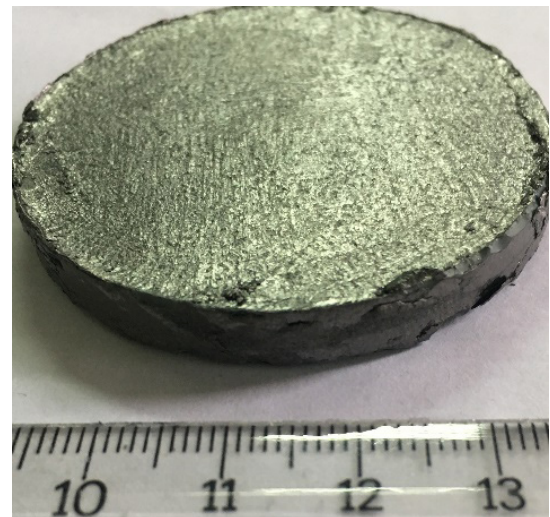
Figure 2. Macro image of the sample produced via SPS process.

2.3. Characterization Methods

The sintering behaviors of the specimens were evaluated by using shrinkage curves obtained from the SPS device. Density of the specimens was determined using Archimedes' principle. Theoretical density values of composites were determined according to the mixture rule and these theoretical values were proportioned to the measured density values. Thus, the relative density values of the composites were calculated (Equation 1).

$$D_R = \frac{D_B}{D_T} \times 100 \qquad (1)$$

In this equation, D_R is the relative density (g/cm³), D_B is the density of the sintered sample (g/cm³) and D_T is the theoretical density. Microstructural and elemental analysis of the samples were performed by using Field Emission Scanning Electron Microscope (FESEM, JEOL JSM 7000F) and Energy Dispersion Spectrometer (EDS – Oxford/Inca), respectively. Phase analysis of the samples were carried out with X-ray diffractometer (XRD, Rigaku Miniflex) using Cu-Kα radiation at a scanning speed of 2°/min at 2θ: 10-80°. In addition, the parts cut from the samples were molded with bakelite and polished in the automatic polishing machine (Metcon) using various levels of sandpaper and piano discs. In the final stages, surface polishing process was applied with 3 μm and 1 μm diamond paste. The hardness of the samples was determined in a Vickers microhardness measuring device (Leica VH-MOT) by applying 12 seconds of action time and 9.8 N load. At least 15 measurements were taken for each sample and both average hardness values and standard deviations were calculated. Fracture toughness measurements of the samples were also carried out using the same hardness device, applying 12 seconds of action time and 19.6 N load. The elasticity modules of the composites were calculated with the rule of mixtures. Fracture toughness values of the samples were calculated by Anstis equation (Equation 2) [13].

$$K_{IC} = k \times \left(\frac{E}{H}\right)^{1/2} \times \left(\frac{P}{c^{3/2}}\right) \qquad (2)$$

here; k is the geometry constant (0.016 ± 0.004), P is the applied load, E is the modulus of elasticity of the composite, H Vickers hardness value and c is half of the average crack length.

3. RESULTS AND DISCUSSIONS

3.1. Densification behavior

The shrinkage curves for the produced samples were given in Figure 3 (a-d). These graphs were plotted as displacement of graphite punches (mm) versus temperature (°C).

During the SPS process, the densification occurring in the powders with the increase of temperature at constant pressure is determined from the displacement amount of the graphite punches due to the shrinkage. After a certain temperature value that is different for each material and composition, the shrinkage is completed and remains constant [6, 8]. Therefore, in order to obtain a dense structure, the sintering temperature should be equal or higher than the temperature at which shrinkage is completed. In this study, the starting and completion temperatures of the shrinkage for monolithic Al_2O_3 and Al_2O_3-nano-SiC composite samples were determined (see Table 2).
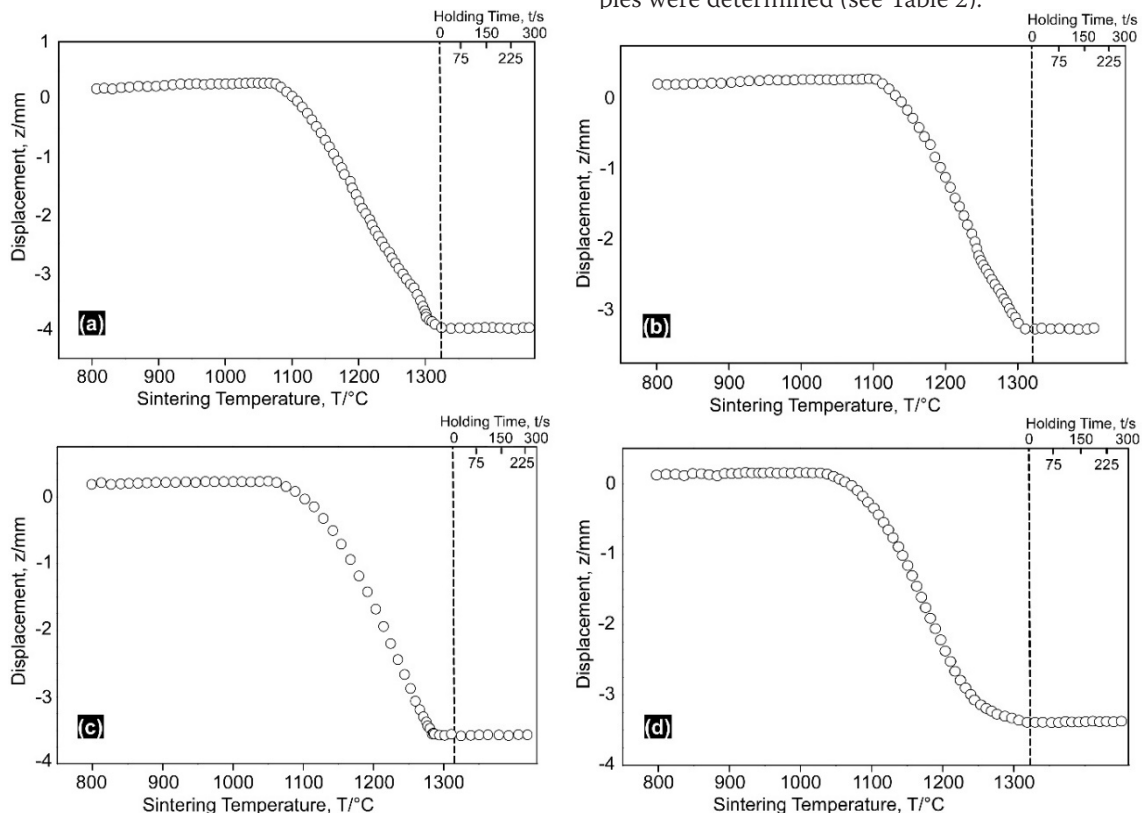
Figure 3. Shrinkage graphs of the samples produced by SPS process, 100A (a), 90A10S (b), 80A20S (c) and 70A30S(d).

Table 2. Starting and completion temperatures of the shrinkage.

Specimen Name	Shrinkage Temperatures (°C)	
	Starting	Completion
100A	1070	1325
90A10S	1105	1305
80A20S	1075	1290
70A30S	1045	1280

As seen in Figure 3 and Table 2, during SPS process performed with a constant heating rate, the starting and completion temperatures of the shrinkage decreased thanks to the nano-SiC added to Al_2O_3. The reason for this decrease occurring in the starting and ending temperatures of sintering was thought to be due to the increase in the conductivity of the composite by SiC, whose electrical conductivity is higher than Al_2O_3. The mechanism of the increase in electrical conductivity of Al_2O_3 by adding SiC has been explained by Saheb at al [2]. As a result, it is possible to conclude that an improvement took place in the sintering behavior of the Al_2O_3 thanks to added nano-SiC particles.

The densities of the specimens produced by the SPS process were determined by Archimedes' Principle. According to the results, it was understood that the relative density values of the specimens varied among 99.7% and 95.2% (see Table 3). The monolithic Al_2O_3 (99.7%) had the highest relative density value among all samples. The lowest relative density value (95.2%) belonged to the specimen of 70A30S sample containing 30% SiC by volume. It was determined that relative density values decreased with increasing nano-SiC ra-

tio. This decrease in density values occurred due to the poor sintering property of the SiC. A similar behavior (decrease in density with increasing SiC ratio added to Al_2O_3) was observed in the study of Alweendo et al. [12].

Table 3. Relative density, hardness and fracture toughness values.

Specimen Name	Relative Density (%)	Hardness (Hv)		Fracture Toughness (K_{Ic})	
		GPa	Std Dev	(MPa·m$^{1/2}$)	Std Dev
100A	99.7	18.27	± 0.73	2.94	± 0.36
90A10S	98.1	21.07	± 0.41	5.81	± 0.43
80A20S	97.2	22.34	± 0.57	6.09	± 0.39
70A30S	95.2	22.83	± 1.10	4.37	± 0.87

3.2. Microstructural Characterizations

FESEM images taken from the fracture surface of the produced specimens using secondary electron detector were given in Figure 4 (a-d). In Figure 4 (b-d), nano-sized SiC grains has been noticed. Especially in Figure 4 (b) and (c), it is seen that the nano-sized SiC grains were homogeneously distributed in the Al_2O_3 matrix. Therefore, it can be said that the ultrasonic nano-SiC dispersion process was successful up to 20% by volume. However, the same homogeneous distribution could not be observed in 70A30S sample containing 30% SiC by volume (Figure 4 (d)). In Figure 4 (a), the microstructure of monolithic Al_2O_3, the coaxial grains were quite distinct and it is understood that there was intergranular fracture. The granular structure in the 70A30S sample was not evident (Figure 4 (d)). This was due to the transgranular fracture. The fracture mode started to transform from intragranular fracture to transgranular fracture
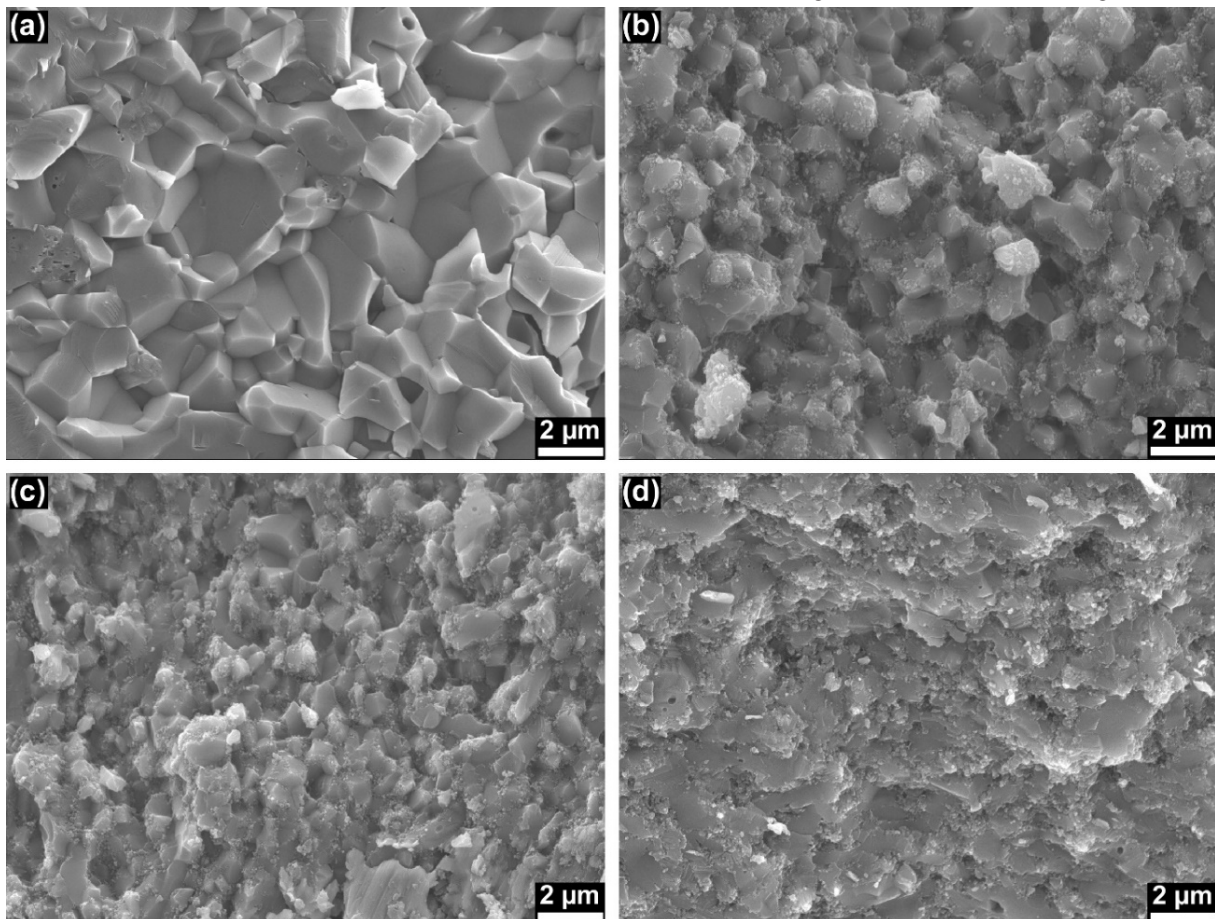
Figure 4. FESEM microstructures of spark plasma sintered specimens; 100A (a), 90A10S (b), 80A20S (c), 70A30S (d).

with the increasing SiC ratio. On the other hand, it is clearly seen that the grain size of the Al_2O_3 matrix decreased with the addition of nano-SiC to the structure. Nano sized SiC particles located around Al_2O_3 grains and prevented the propagation of the grain boundary. Therefore, the grain size of the Al_2O_3 matrix decreased with the nano-SiC addition.

The elemental distributions (by weight) of the EDS spectra taken from the general surface regions of the samples were given in Table 4. In this table, Al, Si, C and O were chemical symbols of aluminum, silicon, carbon and oxygen, respectively. It is understood that the initial powder compositions (by volume → weight) and the values obtained from the EDS results of the produced samples were consistent.

Table 4. Results of elemental analysis

Specimen Name	Weight % Element			
	Al	Si	C	O
100A	62,38	-	-	37,62
90A10S	36,74	4,70	10,41	48,15
80A20S	39,60	10,60	15,84	33,96
70A30S	22,65	12,34	27,42	37,58

3.3. Phase Analysis

In order to understand the phases formed after sintering, XRD analysis were performed and the patterns were given in Figure 5. This process was carried out with an X-ray diffractometer using Cu-Kα radiation at a scanning speed of 2°/min at 2θ: 10-80°. As a result, it was understood that the monolithic Al_2O_3 sample had the structure of α-Al_2O_3 (JCPDS: 71-1683) after SPS process. In case of adding SiC up to 20%, the peaks of the SiC phase appeared and there was no change in the Al_2O_3 structure. However, peaks of the $Al_2Si_2O_5$ phase were revealed in the sample containing 30% SiC by volume.

3.4. Mechanical Properties

Vickers microhardness and fracture toughness values of Al_2O_3-based composites sintered under 40 MPa pressure for 5 min. with the SPS method are given in Table 3. While the hardness value of monolithic Al_2O_3 was 18.27 GPa, it increased to 21.07 GPa with the addition of 10% SiC by volume and 22.34 GPa with the addition of 20% SiC by volume. This was due to the nano-SiC particles preventing dislocation movement during plastic deformation caused by hardness measurement. In addition, increasing in hardness could be explained by the reduction of the grain size of Al_2O_3 matrix by adding nano-SiC to the structure. The grain boundary areas increased with decrease in grain size and these grain boundary areas prevented the movement of dislocations. However, it was determined that the hardness value did not increase any more if 30% SiC by volume was added to the A_2O_3 matrix (22.83 GPa).

As a result of fracture toughness measurements, it was understood that a significant improvement occurred in the fracture toughness value with nano-SiC addition to Al_2O_3 (Table 3). The fracture toughness value of monolithic Al_2O_3, calculated as 2.94 MPa·m$^{1/2}$, increased to 5.81 and 6.09
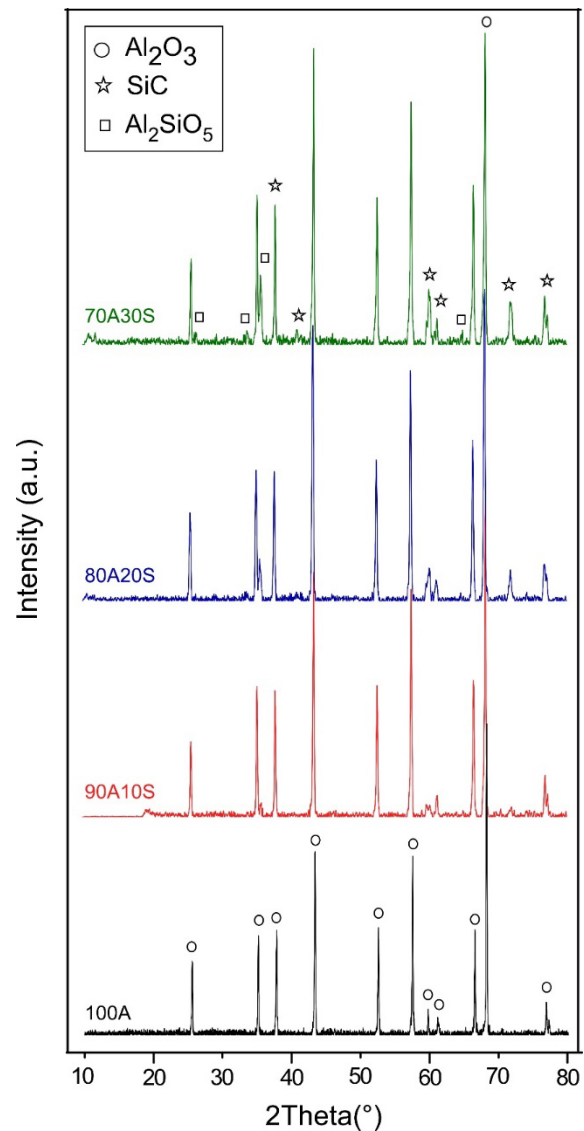
Figure 5. XRD patterns.

MPa·m$^{1/2}$ with the addition of 10% and 20% SiC, respectively. This increase in fracture toughness can be explained by the "Crack Deflection" mechanism caused by nano-sized SiC particles, as Shi et al [14] mentioned. The directions of the cracks propagating in the structure changed when they intersected with the SiC grains and moved in a zigzag pattern (see Figure 6). In this way, the energy of the cracks was reduced and the fracture toughness values of the Al_2O_3-nano SiC composite were improved.

However, the fracture toughness value of Al_2O_3 containing 30% nano-SiC by volume decreased to 4.37 MPa·m$^{1/2}$. A similar decrease in fracture toughness after a certain SiC addition (30% SiC by weight) was observed in a study in the literature [15]. This situation was explained by three mechanisms: (I) high agglomeration of nano-SiC particles occurring at 30% SiC addition (see Figure 7), (II) low fracture toughness of the $Al_2Si_2O_5$ (1-1.8 MPa·m$^{1/2}$ [16]), which formed in the 70A30S sample, (III) excessive residual stresses in the structure as a result of thermal expansion mismatches of Al_2O_3 and SiC. As seen in Figure 7, which is the high magnification SEM image of 70A30S, nano-SiC particles agglomerated in the Al_2O_3 grain boundary regions when 30% nano-SiC by vol-
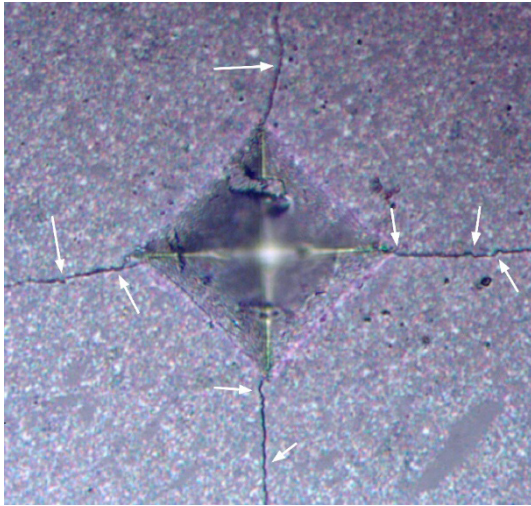
Figure 6. Vickers indentation cracks on the surface of produced Al_2O_3-nano SiC composite.
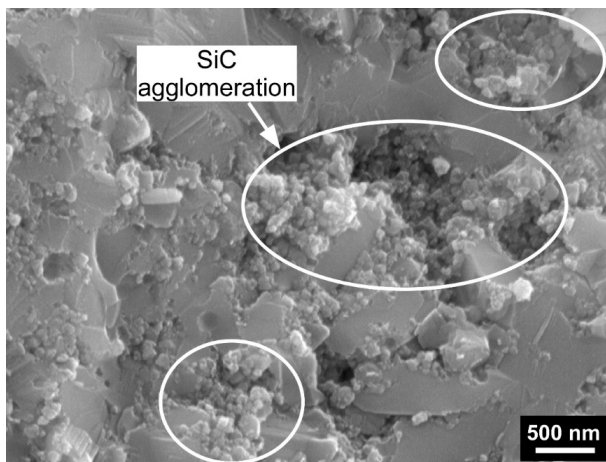
Figure 7. Agglomeration of nano-SiC particles in the grain boundary regions of Al_2O_3.

4. CONCLUSIONS

As a result of the experimental studies, cylindrical shaped Al_2O_3/nano-SiC specimens with a diameter of 50 mm were produced by spark plasma sintering process and their sintering behavior, density, microstructure, phase structure, hardness and fracture toughness were analyzed. According to these analysis:

1. The temperatures at which shrinkage started and completed were decreased with the increasing SiC addition. This situation was explained by the increase in the conductivity of the composite with the increasing SiC addition.

2. The relative density of monolithic Al_2O_3 was 99.7%. However, this value decreased up to 95.2% with the increasing SiC addition.

3. The grain size decreased and the fracture mode changed to transgranular fracture from intergranular fracture with the SiC addition.

4. The hardness increased from 18.27 GPa to 22.83 GPa.

5. While the fracture toughness of the monolithic Al_2O_3 was 2.94 MPa·m$^{1/2}$, a maximum value of 6.09 MPa·m$^{1/2}$ was obtained with the addition of nano-SiC.

6. Addition of 20 vol% SiC was the maximum point for mechanical properties, and over this addition amount the fracture toughness value decreased due to the agglomeration of nano-SiC, excessive residual stress and the formation of $Al_2Si_2O_5$ phase.

REFERENCES

[1] Pravarthana, D., Chateigner, D., Lutterotti, L., Lacotte, M., Marinel, S., Dubos, P.A., et al., (2013). Growth and texture of spark plasma sintered Al2O3 ceramics: A combined analysis of X-rays and electron back scatter diffraction. Journal of Applied Physics. 113(15): 153510. doi: 10.1063/1.4802439.

[2] Saheb, N., Hayat, U., Hassan, S.F., (2019). Recent advances and future prospects in spark plasma sintered alumina hybrid nanocomposites. Nanomaterials. 9(11): 1–43. doi: 10.3390/nano9111607.

[3] Liu, J., Li, Z., Yan, H., Jiang, K., (2014). Spark plasma sintering of alumina composites with graphene platelets and silicon carbide nanoparticles. Advanced Engineering Materials. 16(9): 1111–8. doi: 10.1002/adem.201300536.

[4] Liu, J., Yan, H., Jiang, K., (2013). Mechanical properties of graphene platelet-reinforced alumina ceramic composites. Ceramics International. 39(6): 6215–21. doi: 10.1016/j.ceramint.2013.01.041.

[5] Ahmad, K., Pan, W., (2015). Microstructure-toughening relation in alumina based multiwall carbon nanotube ceramic composites. Journal of the European Ceramic Society. 35(2): 663–71. doi: 10.1016/j.jeurceramsoc.2014.08.044.

[6] Akin, I., (2015). Investigation of the microstructure, mechanical properties and cell viability of zirconia-toughened alumina composites reinforced with carbon nanotubes. Journal of the Ceramic Society of Japan. 123(1437): 405–13. doi: 10.2109/jcersj2.123.405.

[7] Chakravarty, D., Bysakh, S., Muraleedharan, K., Rao, T.N., Sundaresan, R., (2008). Spark plasma sintering of magnesia-doped alumina with high hardness and fracture toughness. Journal of the American Ceramic Society. 91(1): 203–8. doi: 10.1111/j.1551-2916.2007.02094.x.

[8] Ormanci, O., Akin, I., Sahin, F., Yucel, O., Simon, V., Cavalu, S., et al., (2014). Spark plasma sintered Al2O3-YSZ-TiO2 composites: Processing, characterization and in vivo evaluation. Materials Science and Engineering C. 40: 16–23. doi: 10.1016/j.msec.2014.03.041.

[9] Rattanachan, S., Miyashita, Y., Mutoh, Y., (2003). Microstructure and fracture toughness of a spark plasma sintered Al2O3-based composite with BaTiO3 particulates. Journal of the European Ceramic Society. 23(8): 1269–76. doi: 10.1016/S0955-2219(02)00294-7.

[10] Razavi, M., Farajipour, A.R., Zakeri, M., Rahimipour, M.R., Firouzbakht, A.R., (2017). Production of Al2O3-SiC nano-composites by spark plasma sintering. Boletin de La Sociedad Espanola de Ceramica y Vidrio. 56(4): 186–94. doi: 10.1016/j.bsecv.2017.01.002.

[11] Álvarez, I., Torrecillas, R., Solis, W., Peretyagin, P., Fernández, A., (2016). Microstructural design of Al2O3–SiC nanocomposites by Spark Plasma Sintering. Ceramics International. 42(15): 17248–53.

doi: 10.1016/j.ceramint.2016.08.019.

[12] Alweendo, S.T., Johnson, O.T., Shongwe, B.M., Kavishe, F.P., Borode, J.O., (2020). Microstructural and mechanical properties of alumina (Al2O3) matrix composites reinforced with SiC from rice husk by spark plasma sintering. Materials Research. 23(1): 1–9. doi: 10.1590/1980-5373-MR-2019-0363.

[13] Anstis, G.R., Chantikul, P., Lawn, B.R., Marshall, D.B., (1981). A Critical Evaluation of Indentation Techniques for Measuring Fracture Toughness: I, Direct Crack Measurements. Journal of the American Ceramic Society. 64(9): 533–8. doi: https://doi.org/10.1111/j.1151-2916.1981.tb10320.x.

[14] Shi, X.L., Xu, F.M., Zhang, Z.J., Dong, Y.L., Tan, Y., Wang, L., et al., (2010). Mechanical properties of hot-pressed Al2O3/SiC composites. Materials Science and Engineering A. 527(18–19): 4646–9. doi: 10.1016/j.msea.2010.03.035.

[15] Torosyan, K.S., Sedegov, A.S., Kuskov, K. V., Abedi, M., Arkhipov, D.I., Kiryukhantsev-Korneev, P. V., et al., (2020). Reactive, nonreactive, and flash spark plasma sintering of Al2O3/SiC composites—A comparative study. Journal of the American Ceramic Society. 103(1): 520–30. doi: 10.1111/jace.16734.

[16] Whitney, D.L., Broz, M., Cook, R.F., (2007). Hardness, toughness, and modulus of some common metamorphic minerals. American Mineralogist. 92(2–3): 281–8. doi: 10.2138/am.2007.2212.